Visual Abstract

A method and apparatus for characterizing defects in large flat composite structures by Line Scan Thermography and neural network techniques

Arsenii Chulkov, Vladimir Vavilov, Denis Nesteruk
National Research Tomsk Polytechnic University, Russia
chulkovao@tpu.ru
vavilov@tpu.ru, http://orcid.org/0000-0002-9828-7374
nden@tpu.ru

Douglas Burleigh
La Jolla Cove Consulting, USA
ddburleigh@aol.com

Alexey Moskovchenko
University of West Bohemia, Czech Republic
alexeym@ntc.zcu.cz

Abstract. The principle of Line Scan Thermography (LST) was used to develop a self-propelled infrared thermographic nondestructive testing device for the inspection of large, relatively flat composite aerospace parts, such as aircraft wings. The design of the unit allowed the suppression of noise from reflected radiation. Using the LST method, the new equipment, provided defect detectability similar to that achieved with a classic, static, flash heating procedure, but with a higher inspection rate. Also, the line heating principle ensured more uniform thermal patterns, and the proper choice of scan speed and field of view allows the selection of optimal time delays and the creation of maps of defects at different depths. Defect characterization efficiency was improved by using a trained neural network.

Keywords. Infrared Thermography, Line Scan Thermography, Composite Part, Defect Characterization, Neural Network.

OPEN ACCESS

Citation: Chulkov, A., Vavilov, V., Nesteruk, D., Burleigh, D., Moskovchenko, A., A method and apparatus for characterizing defects in large flat composite structures by Line Scan Thermography and neural network techniques, Frattura ed Integrità Strutturale, 63 (2023) 110-121.

Received: 11.07.2022
Accepted: 19.09.2022
Online first: 14.11.2022
Published: 01.01.2023

Introduction

In modern aviation and space technology, many large, complex-shaped parts are made of composite materials, such as carbon fiber reinforced polymer (CFRP) and glass fiber reinforced polymer (GFRP) [1-6]. Nondestructive testing (NDT) of hidden defects in such parts traditionally uses ultrasonic (UT) and X-ray (RT) methods [7-10], and

combinations of some NDT techniques were also proposed, such as laser shearography and thermography [11], eddy current and thermography [12], holographic interferometry and thermography [13]. Inspection during production is usually carried out using complex robotic systems or is performed manually in "field" conditions. Some difficulties in performing the manual NDT of large parts, as well as some difficulties in the application of complex robotic systems, make the development of faster, improved NDT techniques and inspection equipment desirable.

It is important to note that ultrasonic and X-ray testing methods applied to the inspection of composites, have a number of drawbacks, which can be overcome by using thermal non-destructive testing (TNDT) [14]. For example, X-ray testing has very high spatial resolution but is characterized by a low inspection rate, and also requires access to both sides of a test object. In addition, X-ray testing is often ineffective when testing thin-walled composite structures. Practical ultrasonic testing is effective for detecting defects in polymer composites located at depths more than 1-1.5 mm from the surface, but subsurface defects may be located in the so-called "dead zone" and will not be detected. In most cases, this testing method requires the use of a liquid couplant or full immersion of the test object into a liquid. The ultrasonic method is dependent on the surface quality of the test object and typically has a low inspection rate.

The classical TNDT method, which employs optical heat sources such as halogen lamps or Xenon flash lamps, is very good at detecting near-surface defects, at depths up to 4 mm (0,16 inch)) in polymer composites [15, 16]. In addition, this method has a much higher inspection rate than ultrasonic and X-ray testing. The method of ultrasonic infrared thermography (UIT), which uses magnetostrictive or piezoceramic transducers as sources of ultrasonic stimulation, has proven to be efficient for inspecting composite products of complex shape, but has a low inspection rate. UIT best detects the so-called "kissing" (closed) disbonds, whose faces are in a close contact [15]. In 1994, Lehtiniemi and Hartikainen proposed a hand-held inspection device combining a line inductive heater and infrared (IR) scanner thus implementing the concept of Line Scan Thermography (LST) [17, 18]. The principle of induction heating in TNDT was used by Thomas and Balasubramaniam [19]. A portable radio-frequency scanner was described by Salski et al. for inspecting composites [20]. An infrared inspection system called a "thermal photocopier" was proposed by Woolard and Cramer [21]. First, this system was intended for detecting corrosion in boiler tubes [22] and then applied to composite parts [23]. Recently, Khodayar et al. described the methodology of optimization of the LST technique by varying stimulation power and inspection rate [24, 25]. In 2015, Oswald-Tranta and Sorger [26] and, in 2018, Moran and Rajic [27] demonstrated that a principle of phase data treatment can be also used in combination with LST.

To test large flat objects, such as the composite wings of Airbus A350 and MS-21 aircraft, the infrared (IR) LST method can be implemented by using an original portable, robotic flaw detector moving over the surface of the parts being tested. A significant advantage of such an inspection device for the testing of large parts is its flexibility, as it can be used in the laboratory, in manufacturing areas, and in "field" testing. The inspection rate in IR LST testing of large flat test objects depends on the required defect detection depth and defect size, but rates of 20 m^2/hour can be achieved. A self-propelled flaw detector can be guided by automation or under the control of an operator. Data collection and processing can be implemented by using algorithms based on neural networks (NN), thus providing the automated characterization of defect parameters, such as defect depth and size.

In this study, a self-propelled IR thermographic flaw detector was used to inspect defects in multilayer samples that simulated a large flat aircraft part, and the test results were processed using an algorithm based on an artificial NN.

The combination of the LST technique and the NN allowed evaluating defect depth with a reasonable accuracy.

RESEARCH METHOD AND EQUIPMENT

Test samples

For proof of concept testing of the self-propelled LST flaw detector, 13 test samples were manufactured to simulate a multilayer thermal insulation coating on metallic substrates, similar to those that are widely used in the aerospace industry. Inspecting such structures is challenging or impossible for traditional NDT techniques such as ultrasonic and X-ray. In most TNDT studies of composite structures, flat-bottom holes (FBHs) are commonly used to simulate defects. However, in this study, the test panels contained simulated defects of different types, sizes and depths to represent a variety of practical inspection cases.

The test samples (Fig. 1a) were 130 × 300 × 4 mm aluminum alloy (Duralumin D16T) plates. Three layers of 2 mm-thick PMMA (polymethyl methacrylate, also known as acrylic, Plexiglass, Perspex, Lucite, etc.) were adhesively bonded with double-sided cellophane tape (Sellotape) to the aluminum plates. Each PMMA layer was 0.1 mm thick and the tape was 0.01 mm thick. The total thickness of the three layers of PMMA, and three adhesive tape layers, was 6.3 mm, PMMA was chosen

because its thermal diffusivity (1.63×10^{-7} m²/s) is close to that of thermal insulation coatings commonly used in the aerospace industry [28].

Since optical heating was being used, and PMMA is transparent in the optical wavelength, the samples were painted with matte black paint providing a surface absorption coefficient of 0.96 [15].

Each sample plate contained 9 defects, see Fig. 1b. The simulated defects were square FBHs, with lateral dimensions of 5 × 5 mm to 45 × 45 mm, and depths from 0.1 mm to 2 mm. The FBHs were laser machined using a 0.2 mm diameter laser beam, resulting in a depth error of ±0.05 mm.

The arrangement of the simulated defects was the same for each test sample but the depths, relative to the front surface, varied from 1 to 4.2 mm; see Tab. 1. Sample 12 contained no defects. Sample 13 (see Tab. 2) contained 9 defects, the same as the other 11 samples, and this sample was used as the reference for the NN used for data characterization. Details of the manufacturing of the test samples were described in [28].

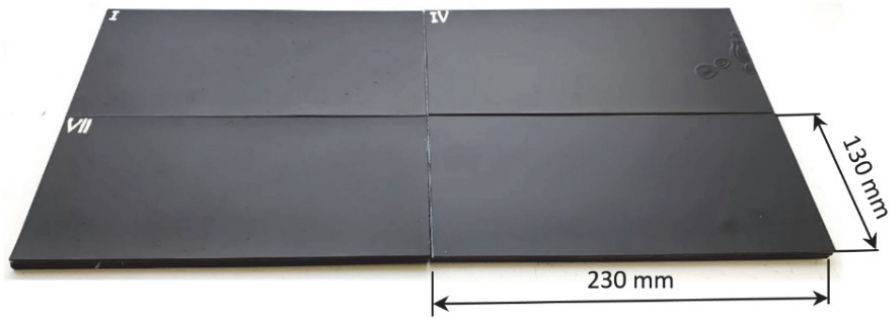

a)

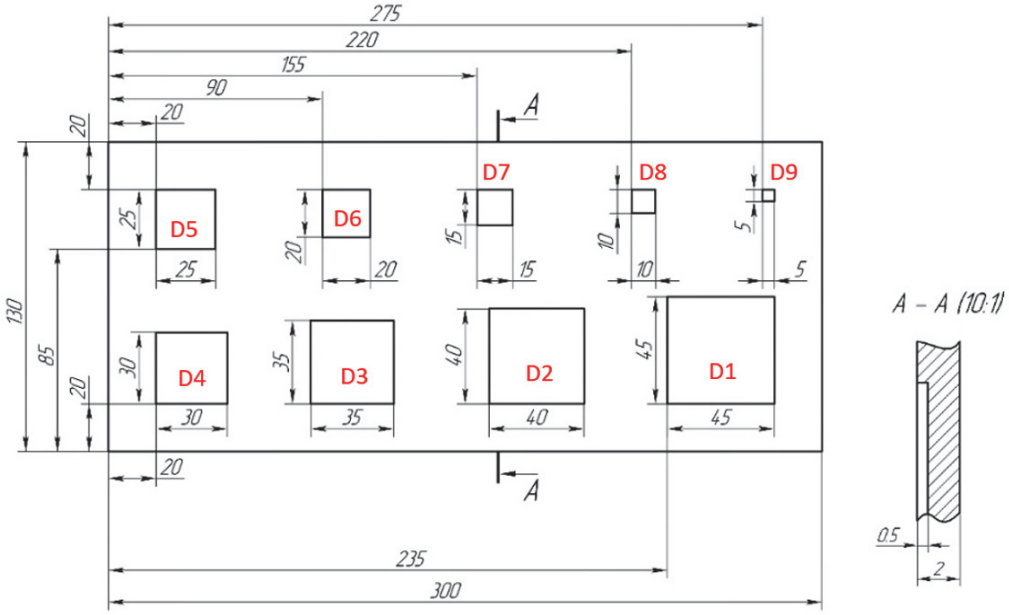

b)

Figure 1: Design of test samples: a) photograph of four test samples (1, 4, 7 and 13); b) defect layout in Sample 3 (example).

Sample	Defect thickness *d*, mm	Defect depth *h*, mm	Sample	Defect thickness *d*, mm	Defect depth *h*, mm
1	1	3.1	7	0.1	2.2
2	1	1	8	0.3	3.8
3	0.5	3.6	9	0.3	1.7
4	0.5	1.5	10	0.3	2.1
5	1.5	2.6	11	0.3	4.2
6	2	2.1	12	No defects	

Table 1: Parameters of defects in test samples.

Defect number	D1	D2	D3	D4	D5	D6	D7	D8	D9
Defect depth *h*, mm	4.0	4.0	3.8	3.8	3.6	3.1	2.6	2.1	2.1
Defect thickness *d*, mm	0.1	0.1	0.3	0.3	0.5	1	1.5	2	2

Table 2: Parameters of defects in test samples.

Allowable defect sizes for large composite aerospace structures are generally in the range of 10 mm (0.4 inch) to 12.7 mm (0.5 inch) [1, 7, 17]. However, in some rare instances, the allowable sizes are as small as 6.4 mm (1/4 inch) or as large as 25 mm (1 inch). The smallest simulated defects in the test samples were 5 × 5 mm. Defects of 45 × 45 mm could be considered as being infinite if the sample thickness is less than a few millimeters. It is worth reiterating that the temperature signals over defects are independent of the defect lateral dimensions if they exceed the defect depth by more than 5-10 times [29, 30]. In this work, the thickness of the test samples was about 6 mm.

Self-propelled LST flaw detector

The newly designed self-propelled LST inspection device includes a 2 kW halogen lamp (optical) heater, an Optris PI640 IR imager, stepper motors and a wireless control system (Fig. 2). The mobile platform rides on rollers, and V-rib drive belts move the device smoothly and prevents the device from "sliding" when moving along a surface with a slight slope.

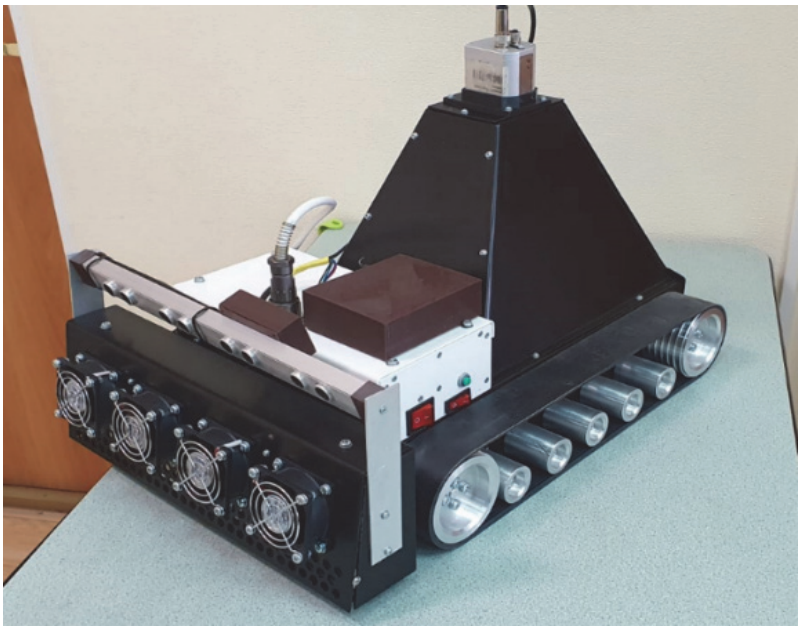

Figure 2: Self-propelled LST flaw detector (Tomsk Polytechnic University).

The basic technical characteristics of the self-propelled flaw detector, and some applications are presented in Tab. 3.

Test procedure

All test samples were arranged in a linear sequence, with the edges of adjacent samples in contact. A laser level was used to assure flatness. The self-propelled LST inspection unit moved over the samples to simulate the testing of a large part (see Fig. 3). The distance from the lower part of the heater reflector to the sample surface was 10 mm and the instantaneous field of view was 500×300 mm

The scan speed of the LST unit was 5 mm/second and this resulted in a scan time of 100 seconds. The distance between the heater and the test zone was 150 mm; therefore, IR thermograms were recorded within a 30-130 second time interval (from the start of heating) by the Optris PI640 IR module. The width of the heating strip L_h was 50 mm, resulting in a heating time of 10 seconds. With this arrangement, the spatial resolution on the sample surface was 0.78 mm, resulting in an acquisition frequency of f = 6.4 Hz, which correctly reconstructs the thermal images of the samples.

Test objects	Large flat parts, made of composite honeycomb sandwich panels, thermal protection coatings, metals
Depth of detected defects, mm	0 – 9*
Minimal lateral size of detected defect, mm	3×3**
Instantaneously tested area, m^2	0.07
Test productivity, m^2/hr	up to 20
Control mode	Manual mode, automated programmed track
Maximal surface temperature of test objects, ^oC	up to 70
Temperature resolution, mK	30
Mass, kg	12
Dimensions, m	0.5×0.4×0.4
Heater type	Halogen lamp, 2 kW
Safe operation zone	Protected by border ultrasonic sensors
Power consumption, kW	2.2

* This parameter depends on material, lateral defect size and thickness, and scan speed.
** For 0.3 mm-thick delamination at 3 mm depth in CFRP (dependent on material, defect depth and lateral size).

Table 3: Technical characteristics of the self-propelled LST flaw detector.

Figure 3: Inspection procedure using the LST device.

Optimizing TNDT test parameters

To determine the optimal parameters of the TNDT of the test samples, a numerical simulation of a one-sided test procedure was carried out by means of the ThermoCalc-3D software (Tomsk Polytechnic University) following the methodology described in [31, 32]. The heating duration was 20 seconds, the heating power was 2000 W/m^2, the time step was 0.2 seconds and the duration of the test was 200 seconds. It is worth pointing out that the simulation took into account additive noise with an amplitude of 0.1°C and multiplicative noise with an amplitude of 5%. The concept of noise in TNDT is described in detail in [15, 33]. Fig. 4 shows the layout of defects for modeling Sample 7. The sample consisted of seven layers of different materials: the 4 mm-thick metal substrate, three 2 mm-thick layers of PMMA each and three layers of the 0.1 mm-thick double-sided Sellotape. The thermophysical properties of the materials used in the simulation are given in Tab. 4.

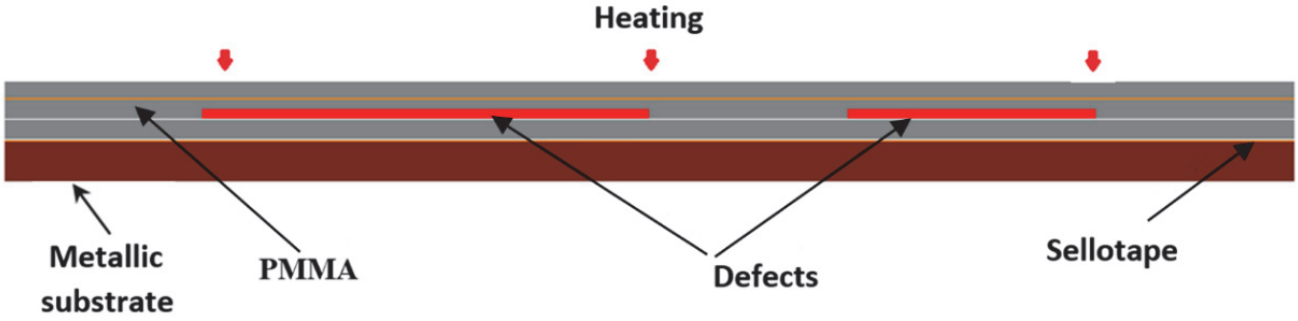

Figure 4: Diagram of the cross-section of Sample 7, showing simulated defects.

Parameter	Aluminum substrate	PMMA	Sellotape	Defect
Thermal conductivity K, W/m·K	177	0.286	0.17	0.02
Heat capacity C, J·kg^{-1}·K^{-1}	875	1524	1100	1030
Density ϱ, kg/m^3	2770	1180	1150	1.1
Thickness L, mm	4	6	0.1	-*

*Defect depth and thickness are shown in Tab. 1.

Table 4: Thermal properties of materials used in numerical stimulation [15].

The modeling results show that the optimum observation times τ_m (the time of the maximum value of the running contrast $C_m = (T_d - T_{nd}) / T_{nd}$, where T_d and T_{nd} are the temperatures in the defect and non-defect areas) are in the range of 24 to 180 seconds, see Tab. 5. Some defects are characterized by calculated C_m values that are lower than 2%, and the corresponding values are not reported in Tab. 5. Note that the TNDT detection limit can be specified, including the noise contrast produced by surface clutter, and it was shown elsewhere that, even with materials that are painted black, the noise threshold is about 2-4% [15].

RESULTS AND DISCUSSION

Experimental results

Taking into account that the field of view of the flaw detector is 500×300 mm, and its scan speed varies from 5 to 50 mm/second, the defects, which can be detected by this device are characterized by an optimal detection time τ_m of 3 to 13 seconds at the scan speed of 50 mm/second and from 30 to 130 seconds at the speed of 5 mm/second. Fig. 5 shows a diagram where dots indicate the values of optimal observation times τ_m of all simulated defects in Samples 1-11 and 13 (numerical data is given in Tab. 5), and the "blue zone" shows the times when a test sample is in the viewed zone

(at the speed of 5 mm/second). Black/red dots show the optimal times for defect detection in Sample 13, which was used as the reference. Note that the points out of the blue area reflect optimal observation times, which are outside of the optimal recording time of the device. However, the corresponding simulated defects can be detected at other delay times.

Test parameters	D1	D2	D3	D4	D5	D6	D7	D8	D9
	Sample 1, d = 1 mm, h = 3.1 mm								
τ_m, s	110	106	119	113	112	99	89	84	-
C_m,%	5.6	5.0	5.1	5.0	5.9	5.5	4.5	3.5	-
	Sample 2, d = 1 mm, h = 1 mm								
τ_m, s	34	34	37	33	31	34	32	29	24
C_m,%	20.1	21.7	21.2	16.4	18.7	23.5	19.3	17.1	4.3
	Sample 3, d = 0.5 mm, h = 3.6 mm								
τ_m, s	119	119	144	148	115	110	109	86	-
C_m, %	3.9	3.5	3.4	3.1	3.6	3.4	3.1	2.3	-
	Sample 4, d = 0.5 mm, h = 1.5 mm								
τ_m, s	34	37	41	39	39	39	41	34	-
C_m,%	9.4	9.9	10.0	11.2	10.5	12.2	12.5	9.0	-
	Sample 5, d = 1.5 mm, h = 2.6 mm								
τ_m, s	116	111	106	102	102	86	81	75	-
C_m,%	7.1	6.7	6.6	6.5	7.4	7.2	6.9	4.8	-
	Sample 6, d = 0.1 mm, h = 4.1 mm								
τ_m, s	76	67	78	74	66	66	60	49	-
C_m,%	13.3	13.0	12.7	11.9	12.5	12.6	11.4	8.8	-
	Sample 7, d = 0.1 mm, h = 2.2 mm								
τ_m, s	104	160	130	130	132	114	112	80	-
C_m,%	1.0	1.3	1.9	1.3	1.2	1.3	1.0	0.7	-
	Sample 8, d = 0.3 mm, h = 3.8 mm								
τ_m, s	125	131	131	124	112	120	116	94	-
C_m,%	3.3	3.4	2.8	3.0	3.4	2.9	2.3	2.0	-
	Sample 9, d = 0.3 mm, h = 1.7 mm								
τ_m, s	39	38	35	39	39	38	37	36	-
C_m,%	8.6	9.4	8.1	8.2	8.5	8.7	8.5	7.3	-
	Sample 10, d = 0.3 mm, h = 2.1 mm								
τ_m, s	47	49	42	51	42	43	43	37	-
C_m,%	5.5	4.9	5.6	5.5	5.4	5.8	5.4	4.1	-
	Sample 11, d = 0.3 mm, h = 4.2 mm								
τ_m, s	137	143	132	180	-	120	102	-	-
C_m,%	2.3	2.6	2.6	2.0	-	2.2	2.0	-	-
	Sample 13**								
τ_m, s	136	111	120	111	108	87	81	47	42
C_m,%	2.2	1.6	1.9	2.0	3.7	6.5	5.0	9.6	3.0

* These defects produce C_m values below the detection threshold of 2%.

** Sample 12 contained no defects. Sample 13 contained 9 defects, the same as the other 11 samples; it was used as the reference when applying the NN for data characterization.

Table 5: Optimal parameters of defect detection in Samples 1-11 and 13 (d - defect thickness, mm) h - defect depth, mm).

Due to the nature of heat diffusion, different TNDT procedures, specifically, area-wide and line-scanning, have similar temperature signals and observation times [32]. In fact, in the scanning mode, these times are slightly shorter than in the case of uniform heating because of higher latent heat diffusion. This allows applying the simulation results for extended period heating to TNDT procedures using moving heat sources.

It is also interesting to consider the possibility of detecting defects whose optimal observation times are out of the experimental time intervals. In the self-propelled LST unit, the largest time interval in which the unit can acquire IR thermograms is from 30 to 130 seconds. However, simulated defects whose optimal detection times are out of this range may still be detected, though the amplitude of the temperature signals will be slightly lower.

Following the discussion above, Fig. 6 shows the IR thermogram of Sample 3 at τ_m =130 seconds obtained by using a classic area-wide TNDT process. It is seen that simulated defects D3 and D4 in this sample are characterized by optimal detection times of 144 and 148 seconds, which are out of the inspection time range of the flaw detector. However, as follows from the image in Fig. 6a, the aforementioned simulated defects can be reliably detected at 130 seconds, and their temperature contrasts remain at about the same level from 120 to 150 seconds. Defect D9 in this sample was not detected, as it had a very low level of temperature contrast. The conclusion above can be also extended on the LST procedure where the flaw detector described above can detect defects beyond the "blue zone" in Fig. 5.

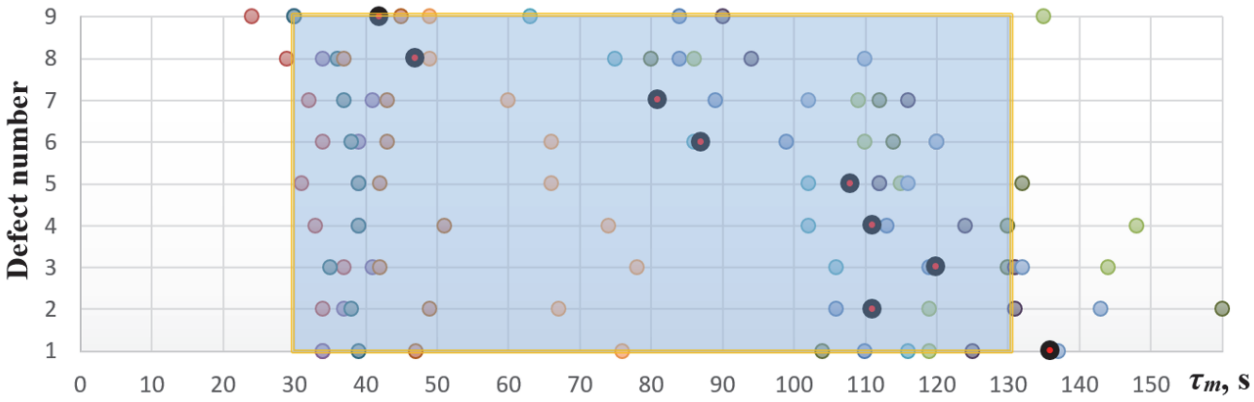

Figure 5: Diagram of optimal observation times (τ_m) for simulated defects in samples and the inspection time range for the self-propelled LST flaw detector (blue area). Each point corresponds to a particular simulated defect (some points are superimposed); the color of the point shows which test sample it represents. The black/red data points correspond to the reference Sample 13.

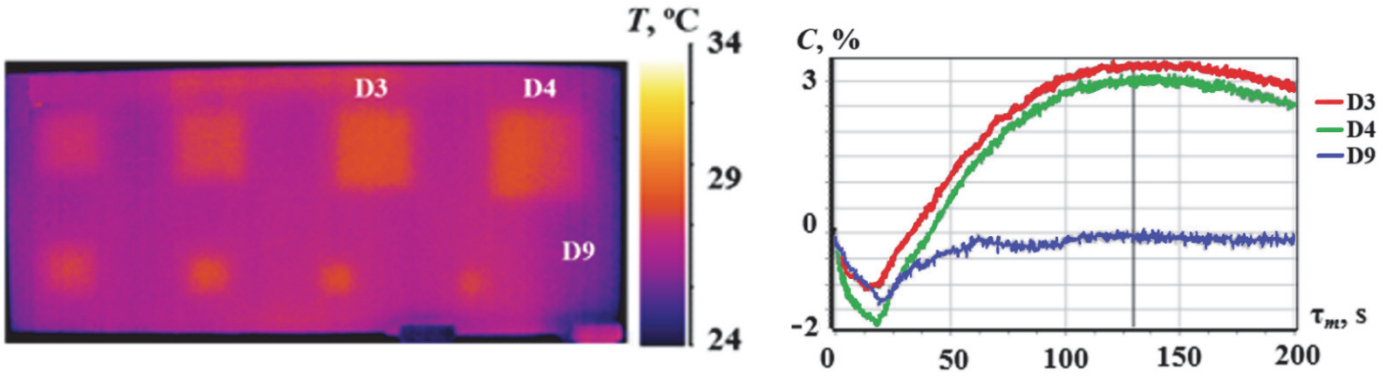

Figure 6: Detecting defects in Sample 3 with non-optimal observation time (classical area-wide TNDT test, observation time 130 seconds).

Fig. 7 shows the panoramic thermogram at 90 seconds of LST testing, obtained after transforming the original sequence as described above and applying a spatial median filter. For convenient analysis, the single raw thermogram was divided into four non-equal images: Samples 12, 13, 1 and 2 were included in the first image. The second image included Samples 3, 4 and 5, the third image included Samples 6-8, and the fourth image included Samples 9-11. Note that there was a time delay in recording thermograms of Samples 6 and 7, and this resulted in the superposition of sample images in the transformed sequence.

It follows from the thermogram in Fig. 7 that some of the samples had natural defects along the perimeters, presumably, disbonds of PMMA and the adhesive tape. In addition, it can be seen that some simulated defects are characterized by an uneven temperature distribution, which is probably associated with a partial separation of PMMA layers near a simulated defect, as well as with the storage of thermal energy above the hollow simulated defects following the heating pulse. This phenomenon is typical for scanned heating. In Samples 12 (defect-free) and 4, some coating deficiencies were simulated, in particular, blistering of the paint (see Fig. 8). Also, some Sellotape markers were applied to the samples for identification.

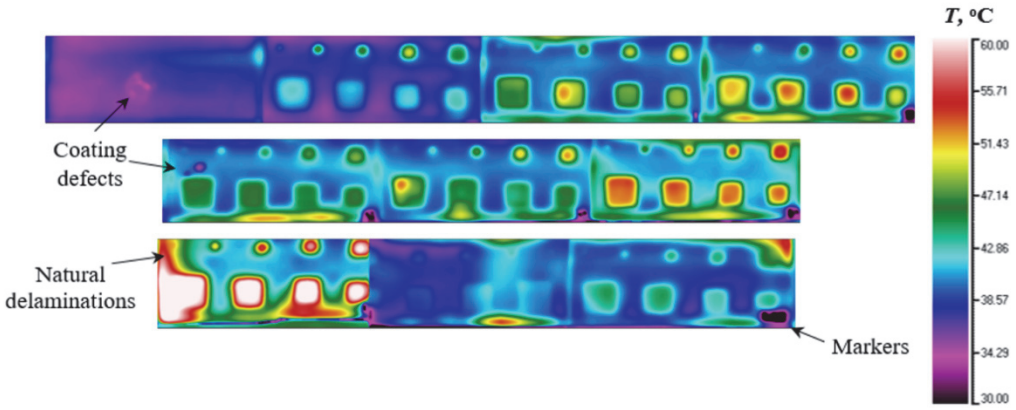

Figure 7: Inspection results (self-propelled LST flaw detector).

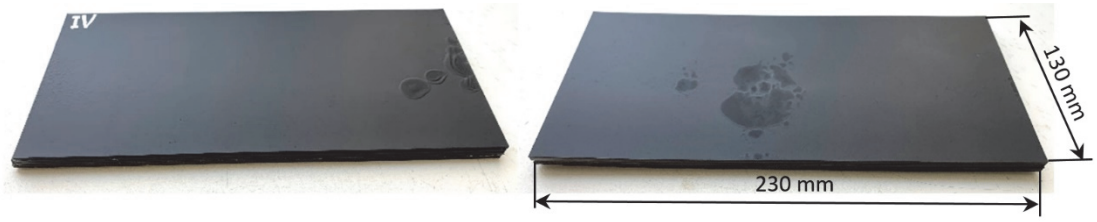

Figure 8: Samples 4 (on the left) and 12 (on the right) with blistered paint.

DATA PROCESSING AND NN TRAINING

The NN was trained only on Samples 1-11, while the defect-free Sample 12 and reference Sample 13 were used to validate characterization results. In the NN training, the time-dependent values of pixel-based temperatures in selected zones were used (an example of NN input temperature profiles is presented in Fig. 9a). Fig. 9b shows the location of zones whose data was used to train the NN. The targets for training the NN were the true values of defect depths (the data is shown in Tab. 1). For defect-free areas, the target was the value of 6 mm, which corresponds to the total thickness of the three PMMA layers.

Before training the NN, the initial sequence of panoramic thermograms was averaged over 4 frames (the initial sequence contained 600 thermograms) and then processed by applying smoothing and median filters). It was found elsewhere that evolving values of the first temperature derivative serve as the best input for training a NN in TNDT because they provide a maximum difference between defect and defect-free areas [34]. The data from 206 zones was used, with an average number of pixels of 350 in each zone. Assuming the number of frames in the sequence was 150, this produced a total of 10,750,000 input values.

The NN contained 5 hidden layers (30, 20, 15, 10 and 1 neurons in particular layers). In the hidden layers, a hyperbolic tangent was used as the activation function, while the output layer realized a linear function for activation. For creating and training the NN, the TensorFlow algorithm set was used, and the NN training quality was estimated by applying a loss function.

It was shown elsewhere that an increase in the number of NN hidden layers improves the accuracy of evaluating the depth of deeper defects [35]. In this study, the criterion for choosing the number of layers was a compromise between the accuracy of defect characterization and computation time. Validation of the proposed defect characterization algorithm was performed on Sample 13 by using the trained NN. Fig. 10 shows the map of defect depths and Tab. 6 shows the retrieved values of defect depths in this sample. The characterization errors were in the range of 6 to 31%, and in the most cases did not exceed 20%l. This is in good agreement with earlier published results [14, 15, 31, 34, 35].

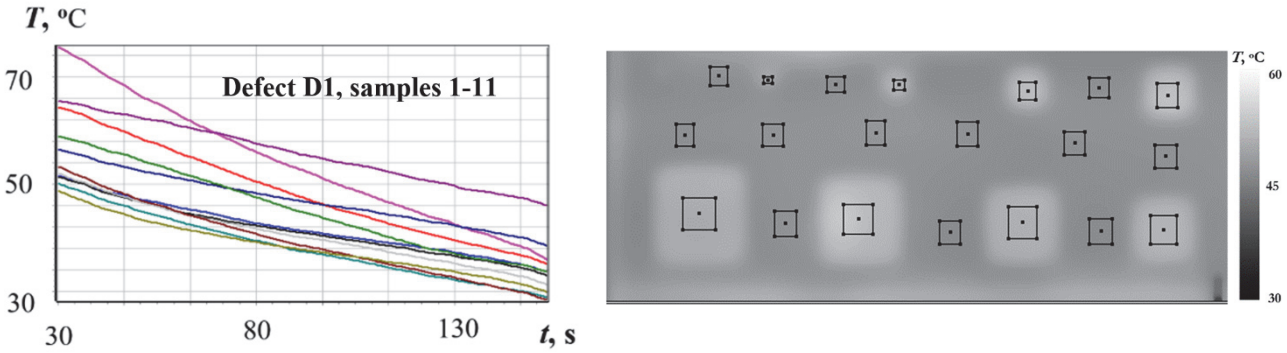

a) b)

Figure 9: NN training: a) temperature evolutions in D1 zones of Samples 1-11 used for NN training, b) IR thermogram of Sample 1 at 90 seconds (the areas shown were used for NN training).

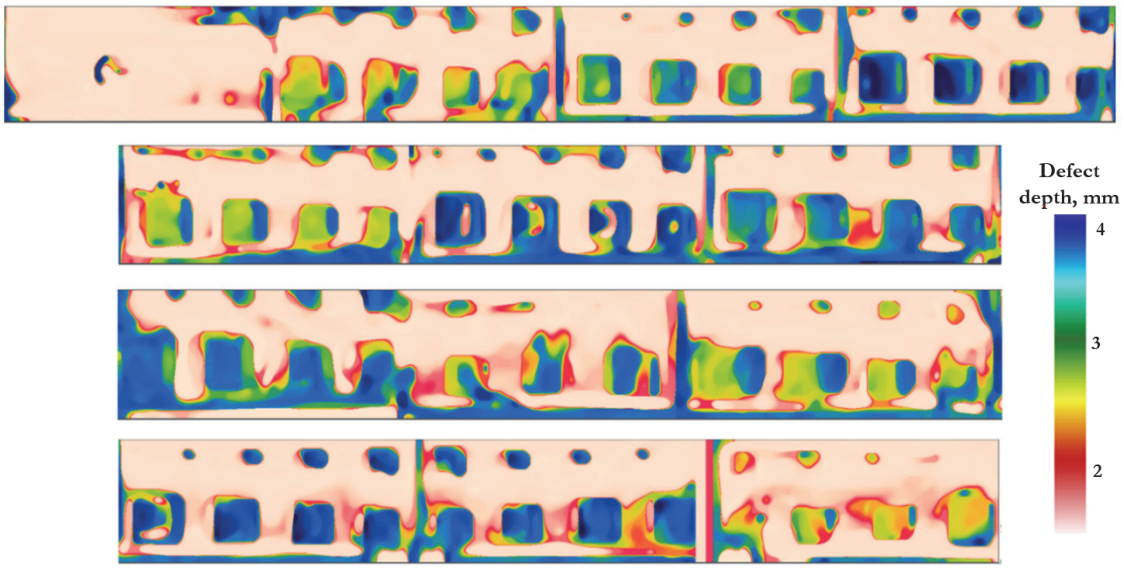

Figure 10: Map of simulated defect depths in Samples 1-13 retrieved by using NN.

Defect number	D1	D2	D3	D4	D5	D6	D7	D8	D9
True defect depth (mm)	4.0	4.0	3.8	3.8	3.6	3.1	2.6	2.1	2.1
Estimated defect depth (mm)	3.33	3.35	3.35	3.25	2.49	2.30	2.13	1.97	1.86
Error (%)	17	16	12	14	31	26	18	6	11

Table 6: Characterizing simulated defect depths in the reference Sample 13.

Conclusion

- The LST technique has been implemented in an original self-propelled TNDT device for inspecting large flat objects, such as aircraft wings, in laboratory or field conditions.
- It is believed that a modified version of this unit would allow the suppression of reflected radiation noise because of the separation between the heated and monitored areas.
- The use of the LST technique and the self-propelled equipment provided defect detectability similar to that of a classic flash heating TNDT technique, but with a much higher inspection rate. This rate could be as high as 20 m²/hour per hour.

- The line heating process ensured more uniform thermal patterns, and the proper choice of scan speed and field of view allows the selection of optimal time delays and the creation of maps of defects at different depths.
- Defect detection efficiency was improved by using a trained NN where temperature derivatives served as input values. This allowed the determination of defect depth with an accuracy of 6 to 31%.
- Future work will validate the effectiveness of the self-propelled TNDT device in laboratory conditions.
- Following that, we will work towards implementing LST as an inspection technique in the aerospace industry.

ACKNOWLEDGMENTS

This study was supported by the Russian Scientific Foundation grant 22-29-01469.

REFERENCES

[1] Gholizadeh, S. (2016). A review of non-destructive testing methods of composite materials, Procedia Structural Integrity, 1, pp. 50-57. DOI: 10.1016/j.prostr.2016.02.008.
[2] Mrazova, M. (2013). Advanced composite materials of the future in aerospace industry, INCAS Bulletin, 5 (3), pp. 139-150. DOI: 10.13111/2066-8201.2013.5.3.14.
[3] Hagnell, M.K., Kumaraswamy, S., Nyman, T., Åkermo, M. (2020). From aviation to automotive - a study on material selection and its implication on cost and weight efficient structural composite and sandwich designs, Heliyon, 6 (3), e03716. DOI: 10.1016/j.heliyon.2020.e03716.
[4] Vlasova, V. (2019). Using composite materials in aircraft, AIP Conference Proceedings, 2171, 030020. DOI: 10.1063/1.5133186.
[5] Karthigeyan, P., Senthil, Raja M., Hariharan, R., Karthikeyan, R., Prakash, S. (2017). Performance evaluation of composite material for aircraft industries, Materials Today: Proceedings, 4 (2), Part A, pp. 3263-3269.
[6] Bing Wang, Shuncong Zhong, Tung-Lik Lee, Fancey K., Mi J. (2020). Non-destructive testing and evaluation of composite materials/structures: A state-of-the-art review, Advances in Mechanical Engineering, Febr. 2020. DOI: 10.1177/1687814020913761.
[7] Li, H., Zhou, Z. (2017). Air-coupled ultrasonic signal processing method for detection of lamination defects in molded composites, J. Nondestruct. Eval., 36, pp. 45-52. DOI: 10.1007/s10921-017-0425-5.
[8] Kinra, V.K., Ganpatye, A.S., Maslov, K. (2006). Ultrasonic ply-by-ply detection of matrix cracks in laminated composites, J. Nondestruct. Eval., 25, pp. 37–49. DOI: 10.1007/s10921-006-0001-x.
[9] Littles, J.W., Jacobs, L.J., Zureick, AH. (1998). Single-sided ultrasonic technique to characterize thick FRP composites, J. Nondestr. Eval., 17, pp. 223–230. DOI: 10.1023/A:1022628705782.
[10] Pomarède, P., Meraghni, F., Peltier, L., Delalande, S., Declerq, N. (2018). Damage evaluation in woven glass reinforced polyamide 6.6/6 composites using ultrasound phase-shift analysis and X-ray tomography, J. Nondestruct. Eval., 37(1), pp. 12-21. DOI: 10.1007/s10921-018-0467-3.
[11] Fröhlich, H.B., de Oliveira, B.C.F., Gonçalves, A.A. (2021). Estimation of impact energies in composites using an out-of-distribution generalization of stacked models trained with shearography and thermography images, J. Nondestruct. Eval., 40 (72). DOI: 10.1007/s10921-021-00809-2.
[12] Tsopelas, N., Siakavellas, J. (2006). Electromagnetic-thermal NDT in thin conducting plates, NDT & E Intern., 39 (5): 391-399. DOI: 10.1016/j.ndteint.2005.11.002.
[13] Theodorakes, P., Ibarra-Castanedo, C., Sfarra, S., Avdelidis, N.P., Maldague, X., Paoletti, D., Ambrosini, D. (2012). NDT inspection of plastered mosaics by means of transient thermography and holographic interferometry, NDT & E Intern., 47, pp.150-156. DOI: 10.1016/j.ndteint.2012.01.004.
[14] Montinaro, N., Cerniglia, D., Pittaresi, G. (2018). Evaluation of interlaminar delaminations in titanium-graphite fibre metal laminates by infrared NDT techniques, NDT & E Intern., 98, pp. 134-146. DOI: 10.1016/j.ndteint.2018.05.004.
[15] Vavilov, V., Burleigh, D. (2019). Infrared thermography and thermal nondestructive testing, Switzerland, Springer Cham. DOI: 10.1007/978-3-030-48002-8.
[16] Infrared thermography in the evaluation of aerospace composite materials. Eds. C. Meola, S. Boccardi, G. Carlomagno. (2016). Elsevier Science, 180 p., ISBN 9781782421719.

[17] Lehtiniemi, R, Hartikainen, J. (1994). An application of induction heating for fast thermal non-destructive evaluation, Rev. of Sci. Instr., 65 (6), 2099. DOI: 10.1063/1.1144818.
[18] Ley O., Butera M., Godinez V. Inspection of composite structures using linescanning thermography. (2012). Proceedings of SPIE - The International Society for Optical Engineering, May 2012. DOI: 10.1117/12.919176.
[19] Thomas, K.R., and Balasubramaniam, K. (2015). Scanning induction thermography (SIT) for imaging damages in carbon-fibre reinforced plastics (CFRP) components, AIP Conference Proc., 1650(1), DOI: 10.1063/1.4914624.
[20] Salski, B., Gwarek, W., Kopyt, P., Theodorakeas, P., Hatziioannidis, I., Koui, I., Alvin Yung Boon Chong, Shu-Mei Tan, Kappatos, V., Selcuk, C., Tat-Hean Gan. (2016). Portable automated radio-frequency Scanner for non-destructive testing of carbon-fibre-reinforced polymer composites, J. Nondestruct. Eval., 35(25). DOI: 10.1007/s10921-016-0343-y.
[21] Woolard, D.F., Cramer, K.E. (2004). The thermal photocopier. A new concept for thermal NDT, Proc. SPIE, Thermosense-XXVI, 5405. DOI: 10.1117/12.541881.
[22] Cramer, K.E., Jacobstein, R., Reilly, T. (2001). Boiler tube corrosion characterization with a scanning thermal line, Proc. SPIE "Thermosense XXIII", 4360, pp. 594-605.
[23] Woolard, D.F., Cramer, K.E. (2005). Line scan versus flash thermography: Comparative study on reinforced carbon-carbon, Proc. SPIE "Thermosense-XXVII", 5782. DOI: 10.1117/12.603789.
[24] Khodayar, F,, López, F. Ibarra-Castanedo, C. Maldague. X. (2017). Optimization of the Inspection of Large Composite Materials Using Robotized Line Scan Thermography, Materials Science, J. Nondestr. Eval., 36(32). DOI: 10.1007/S10921-017-0412-X.
[25] Khodayar, F., Lopez, F., Ibarra-Castaneda, C., Maldague, X. (2018). Parameter optimization of Robotized Line Scan thermography for CFRP composite inspection, J. Nondestr. Eval., 37(1). DOI: 10.1007/s10921-017-0459-8.
[26] Oswald-Tranta, B., Sorger, M. (2012). Scanning pulse phase thermography with line heating, QIRT J., 9(2). DOI: 10.1080/17686733.2012.714967.
[27] Moran, J., Rajic, N. (2018). Remote Line Scan Thermography for the rapid inspection of composite impact damage. Composite Structures, October 2018, 208 (4). DOI:10.1016/j.compstruct.2018.10.038.
[28] Chulkov, A.O., Vavilov, V.P., Moskovchenko, A.I. (2019). Active thermal testing of delaminations in heat-shielding structures, Rus. J. Nondestruct. Testing, 55(3), pp. 240-247. DOI: 10.1134/S1061830919030033.
[29] Zeng Z., Li C., Tao N., Feng L., Zhang C. (2012). Depth prediction of non-air interface defect using pulsed
[30] Thermography, NDT E Int., 48, pp. 39–45, Jun. 2012, DOI: 10.1016/j.ndteint.2012.02.008.
[31] Sirikham A., Zhao Y., and Mehnen J. (2017). Determination of thermal wave reflection coefficient to better estimate defect depth using pulsed thermography. Infrared Phys. Technol., 86, pp. 1–10, DOI: 10.1016/j.infrared.2017.08.012.
[32] Peeters, J., Ibarra-Castanedo, C., Sfarra, S., Maldague, X., Dirckx, J. J. J., Steenackers, G. (2017). Robust quantitative depth estimation on CFRP samples using active thermography inspection and numerical simulation updating, NDT & E Intern., 87, pp. 119-123. DOI: 10.1016/j.ndteint.2017.02.003.
[33] Chulkov, A.O., Tuschl, C., Nesteruk, D.A., Oswald-Tranta, B., Vavilov, V.P., Kuimova, M.V. (2021). The detection and characterization of defects in metal/non-metal sandwich structures by thermal NDT, and a comparison of areal heating and scanned linear heating by optical and inductive methods, J. Nondestruct. Eval., 40(44). DOI: 10.1007/s10921-021-00772-y.
[34] Marani, R., Palumbo, D., Galietti, U., Stella, E., D'Orazio, T. (2019). Enhancing defects characterization in pulsed thermography by noise reduction, NDT & E Intern., 102. DOI: 10.1016/j.ndteint.2018.12.009.
[35] Chulkov, A.O., Nesteruk, D.A., Vavilov, V.P., Saeed, N., Omar, M. (2019). Optimizing input data for training an artificial neural network used for evaluating defect depth in infrared thermographic nondestructive testing, Infr. Phys. & Techn., 102(103047). DOI: 10.1016/j.infrared.2019.103047.
[36] Numan, S., Omar, M.A., Abdulrahman, Y., Saed, A. (2019). Experimentally validated defect depth estimation using artificial neural network in pulsed thermography, Infr. Phys. & Techn., 98. DOI: 10.1016/j.infrared.2019.03.014.